

Generating Patient-like Phantoms Using Fully Unsupervised Deformable Image Registration with Convolutional Neural Networks

Junyu Chen, Ye Li, Eric C. Frey

Russell H. Morgan Department of Radiology and Radiological Science, Johns Hopkins Medical Institutes, Baltimore, MD, USA
Department of Electrical and Computer Engineering, Johns Hopkins University, Baltimore, MD, USA

The use of Convolutional neural networks (ConvNets) in medical imaging research has become widespread in recent years. However, a major drawback of these methods is that they require a large number of annotated training images. Data augmentation has been proposed to alleviate this. One data augmentation strategy is to apply random deformation to existing image data, but the deformed images often will not follow exhibit realistic shape or intensity patterns. In this paper, we present a novel, ConvNet based image registration method for creating patient-like digital phantoms from the existing computerized phantoms. Unlike existing learning-based registration techniques, for which the performance predominantly depends on the domain-specific training images, the proposed method is fully unsupervised, meaning that it optimizes an objective function independently of training data for a given image pair. While classical methods registration also do not require training data, they work in a lower-dimensional parameter space; the proposed approach operates directly in the high-dimensional parameter space without any training beforehand. In this paper we show that the resulting deformed phantom competently matches the anatomy model of a real human while providing the "gold-standard" for the anatomies. Combined with simulation programs, the generated phantoms could potentially serve as a data augmentation tool in today's deep learning studies.

Index Terms—Image Registration, Computerized Phantom, CT, Convolutional Neural Networks

I. INTRODUCTION

COMPUTERIZED phantoms for nuclear medicine imaging research have been built based on anatomical and physiological models of human beings. They have played a crucial part in evaluation and optimization of medical imaging techniques and image reconstruction, processing and analysis methods [1]–[4]. Since the exact structural and physiological properties of the phantom are known, they can serve as a gold standard for the evaluation and optimization process. The 4D extended cardiac-torso (XCAT) phantom [5] was developed based on anatomical images from the Visible Human Project data. This realistic phantom includes parameterized models for anatomy, which allows the generation of different anatomical variations of the phantom. These phantoms have been used in Nuclear Medicine imaging researches [6]–[8], as well as in the various applications of deep learning [9]–[11]. By changing the values of parameters that control organ anatomy, the volumes and shapes of some tissues can be varied. However, the scaling of organs, even when different factors are used in orthogonal directions, does not fully and truly capture the interior anatomical variations within different patients. In [12], Segars et al. used a deformable image registration technique to map phantom labels to patient segmentation; the resulting deformation fields were then being applied to the phantom, thus creating a population of the new XCAT models that capture the anatomical variability among patients. This method relies on the segmentation of patient images, which is tedious and time consuming. In this work, we propose a Convolutional Neural Networks (ConvNets) based approach to perform patient to patient registration. The resulting deformation field can then be applied to organ label maps to automatically generate a segmentation of the patient image.

Deformable Image registration is a process of transforming two images into a single coordinate system, where one image is often referred to as the moving image, we denote it as I_m , while the other is referred to as the fixed image, denoted as I_f . Traditional methods formulate registration as a variational problem for estimating a smooth mapping, ϕ , between the points in one image and those in another. They often tend to iteratively minimize the following energy function (eq. 1) on a single image pair [13]:

$$E = E_{sim}(I_m \circ \phi, I_f) + R(\phi), \quad (1)$$

where, E_{sim} measures the level of alignment between the transformed moving image, $I_m \circ \phi$, and the fixed image, I_f . Some common choices for E_{sim} are mean squared error (MSE) or the L^2 norm of the difference [14], sum of squared differences (SSD) [15], cross-correlation (CC) [16], and mutual information (MI) [17]. The transformation, ϕ , at every point is defined by an identity transformation with the displacement field \mathbf{u} , or $\phi = Id + \mathbf{u}$, where Id represents the identity transform [18]. The second term, $R(\phi)$, is referred to as the regularization on the deformation, ϕ , which enforces the spatial smoothness. It is usually characterized by the gradients of \mathbf{u} . One common assumption is that similar structures are presented in both moving and fixed images. Hence, a continuous and invertible deformation field (a diffeomorphism) is more desired, and the regularization term, $R(\phi)$, was designed for such reason. While diffeomorphisms are essential in some studies, for which the registration field is analyzed further. In the application of registration-based segmentation, the quality of the segmentation propagation is more critical than the diffeomorphic property of the underlying deformation fields [19]. In this study, due to the large interior and exterior shape

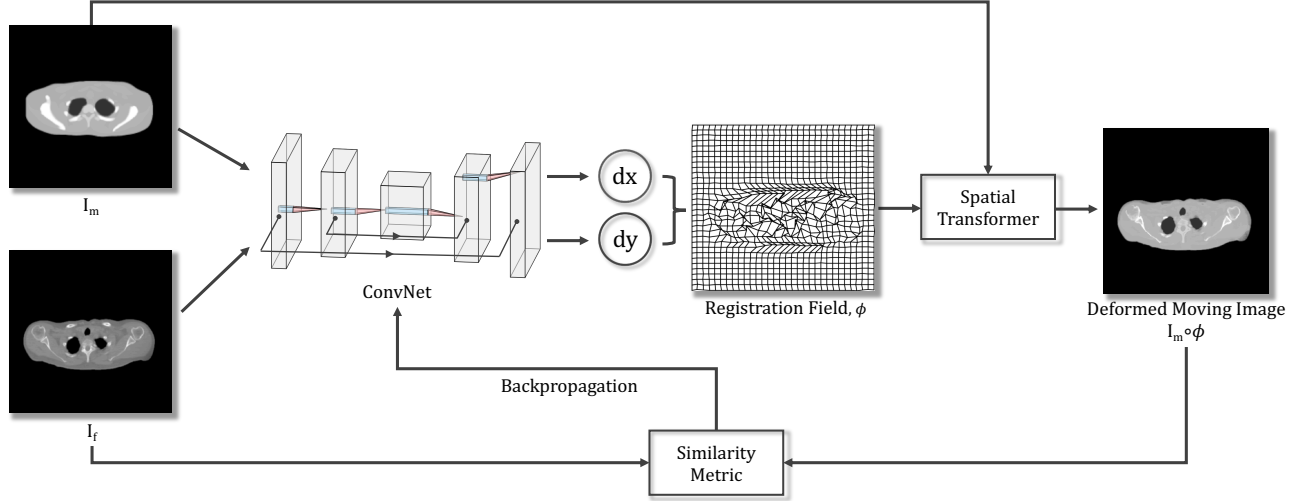


Fig. 1: Schematic of the proposed method. The network takes a pair comprised of one moving and one fixed image as its inputs. The ConvNet learns from a single image pair and generates a deformation field, ϕ . We then warp the moving image I_m with ϕ using a B-spline spatial transformer. The loss determined by the image similarity measure between $I_m \circ \phi$ and I_f was backpropagated to update the parameters in the ConvNet. Since no aspect of the ConvNet is learned from a prior training stage, our method follows a fully unsupervised paradigm.

variability between digital phantoms and patients, we did not impose the registration to be diffeomorphic.

Recently, many deep learning-based methods were proposed to perform the registration tasks, for instance, [18], [20]–[23]. Some of the listed methods were introduced as the unsupervised (or more precisely, self-supervised) techniques, but they still require a prior training stage with a large amount of training data. These methods assume that neural networks could learn the universal computation of the displacement field by minimizing the registration energy function over a dataset of images. This is a common assumption to make with the deep learning based approach. Yet, such an assumption could be unreliable according to a recent study from Zhang et al. [24], where they showed that a well-generalized CNN classifier trained by a large dataset can still easily overfit a random labeling of the training data. More studies on fooling the deep neural networks (DNNs) with adversarial images also suggested that the well-trained networks can be unstable to small or even tiny perturbations of the data [25]–[29]. Whereas, our proposed registration method is fully unsupervised, meaning that ***no previous training is required***. Instead of following the conventional pattern of training a network on a huge dataset of accurately annotated images, we show that CNN is able to estimate an optimal deformation field for a single image pair by minimizing the energy function described in eq. 1 iteratively. This idea was inspired by Lempitsky et al.’s work on the Deep Image Prior [30] (DIP), where they found that learning from a large amount of data is not necessary for building useful image priors, but the structure of a convolutional generator network itself is sufficient to capture plenty of image statistics. They treated the training of ConvNets with random initialization as a regularization prior, in order to achieve good solutions in their application of image denoising, determining early stopping points are often

required. Whereas in image registration, instead of starting from a random initialization (i.e., random noises), it makes logical sense to initialize the ConvNet with moving images. Since one would like to make a moving image as similar to a target image as possible, an early stopping is not desired. In this work, we treat ConvNet as an optimization tool, where it minimizes the energy function via reparametrization in each iteration.

II. METHOD

A. Computerized Phantom Generation

The phantom used in this study was created on the 3D attenuation distributions of the realistic NURBS-based XCAT phantom [31]. Attenuation values were computed based on the material compositions of the materials and the attenuation coefficients of the constituents at 140 keV, the photon energy of Tc-99m used in Nuclear Medicine. Only a single 3D phantom image was used to be deformed to multiple patient CT image. Simulated attenuation map image can be treated as the template image, and phantom image can then be think of as the atlas in the traditional paradigm of medical image registration. Our aim is to register phantom image to patient CT images for the segmentation of patient scans and creating patient-like phantoms.

B. Image Registration with ConvNet

Let a moving image be I_m , and a fixed image be I_f , we assume that they are 2D grayscale images and affinely aligned. We model the computation of the displacement field, ϕ , given the image pair, I_m and I_f , using a deep ConvNet with its parameters θ , i.e., $f_\theta(I_m, I_f) = \phi$. Figure 1 describes the architecture of our proposed method, it consists of a ConvNet that outputs registration field, and a B-spline spatial

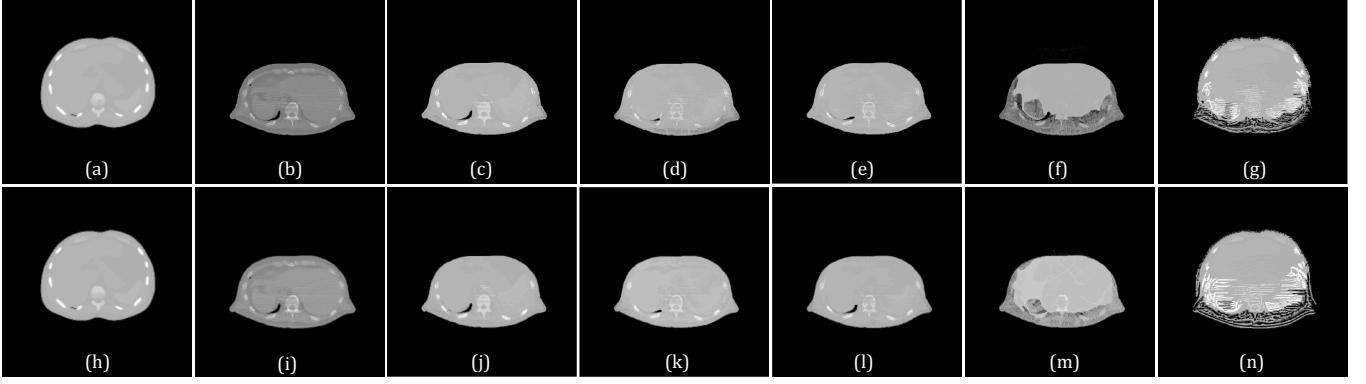


Fig. 3: Comparison of registered XCAT phantom image generated by different loss functions. (a) and (h) One example slice of XCAT phantom image as moving image, I_m . (b) and (i) Patient CT image, later was blurred with Gaussian filter ($\sigma = 0.8$) to reduce beam hardening artifacts. It was used as fixed image, I_f . Third column to the last column are registration results from different loss functions: (c) and (j) PCC. (d) and (k) SSIM. (e) and (l) CC+SSIM. (f) and (m) MSE. (g) and (n) CC.

is more desired, we can define the loss function to be:
 $\mathcal{L}_{sim}(I_m, I_f, \phi; \theta) = 1 - \text{PCC}(I_m \circ \phi, I_f)$.

c) Local Cross Correlation (CC)

Another popular image similarity metric is CC, for its robustness to intensity variations between images, it can be formulated as follows [16], [22], [34]:

$$\text{CC}(I_d, I_f) = \sum_{p \in \Omega} \frac{(\sum_{p_i} (I_f(p_i) - \bar{I}_f(p)) (I_d(p_i) - \bar{I}_d(p)))^2}{\sum_{p_i} (I_f(p_i) - \bar{I}_f(p)) \sum_{p_i} (I_d(p_i) - \bar{I}_d(p))}, \quad (7)$$

where I_d is the deformed image (i.e., $I_m \circ \phi$), p_i represents the pixel location within a window p , and \bar{I}_f and \bar{I}_d denote the local mean intensities within the window. Since $\text{CC} \geq 0$, we minimize the negative CC. Then, the loss function is $\mathcal{L}_{sim}(I_m, I_f, \phi; \theta) = -\text{CC}(I_m \circ \phi, I_f)$.

d) Structural Similarity Index (SSIM)

SSIM was first introduced in [35] for robust image quality assessments based on the degradation of structural information. Within a given image window, SSIM is defined by:

$$\text{SSIM}(I_d, I_f) = \frac{(2\mu_{I_d}\mu_{I_f} + C_1)(2\sigma_{I_f I_d} + C_2)}{(\mu_{I_f}^2 + \mu_{I_d}^2 + C_1)(\sigma_{I_f}^2 + \sigma_{I_d}^2 + C_2)}, \quad (8)$$

where C_1 and C_2 are small constants for avoiding instability, μ_{I_f} and μ_{I_d} , and σ_{I_f} and σ_{I_d} are local means and standard deviations of the image I_f and I_d , respectively. SSIM has a range from -1 to 1, where 1 indicates a perfect structural similarity. Thus, $\mathcal{L}_{sim}(I_m, I_f, \phi; \theta) = 1 - \text{SSIM}(I_m \circ \phi, I_f)$.

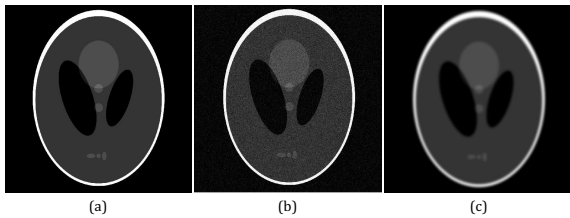


Fig. 4: Comparison of "Shepp-Logan" phantom images [36] with different types of distortions. (a) Original Image. (b) Image corrupted by Gaussian noise. SSIM: 0.14, PCC: 0.96. (c) Gaussian blurred image. SSIM: 0.9, PCC: 0.94.

e) PCC + SSIM

While PCC is robust to noises, it was also found to be less sensitive to blurring. A motivating example is shown in Figure 4, where in (b), the Shepp-Logan phantom image [36] was corrupted with Gaussian noise, and in (c), the image was blurred by a Gaussian filter. Both (b) and (c) yield a lower SSIM and a higher PCC. If we think of (a) as moving image, and (b) and (c) as fixed images, SSIM would impose the ConvNets to model the details, including noises and artifacts. Whereas, using PCC alone as the loss function might converge to a blurred result. Hence, there is a need to balance those two similarity measures. Fortunately, both PCC and SSIM are bounded with a range from -1 to 1, where 1 means the most similar. Thus, we propose to combine SSIM and PCC by an equal weight:

$$\mathcal{L}_{sim}(I_m, I_f, \phi; \theta) = 0.5 * (1 - \text{SSIM}(I_m \circ \phi, I_f)) + 0.5 * (1 - \text{PCC}(I_m \circ \phi, I_f)) \quad (9)$$

C. Registration Procedure

The algorithm for the proposed method is shown in Algorithm 1. For a given pair of moving and fix image, I_m and I_f , an untrained ConvNet (f_θ) was initialized. First, the untrained f_θ produces an initial deformation field, ϕ . Second, we deform the moving image by ϕ (i.e., $I_m \circ \phi$). Then, the loss between I_d and I_f is computed for the use of updating the parameters in the f_θ . The above procedure is repeated until we hit the maximum number of iterations.

Since no information other than the given image pair is needed, the proposed method requires no previous training, thus it is fully unsupervised. The ConvNet is capable of learning an "optimal" deformation from a single pair of image. In the next section, we discuss the performance comparisons between this method and the state-of-the-art unsupervised methods.

III. EXPERIMENTS

We aim to create patient-like phantoms by registering the existing XCAT phantom with patient CT images. There were

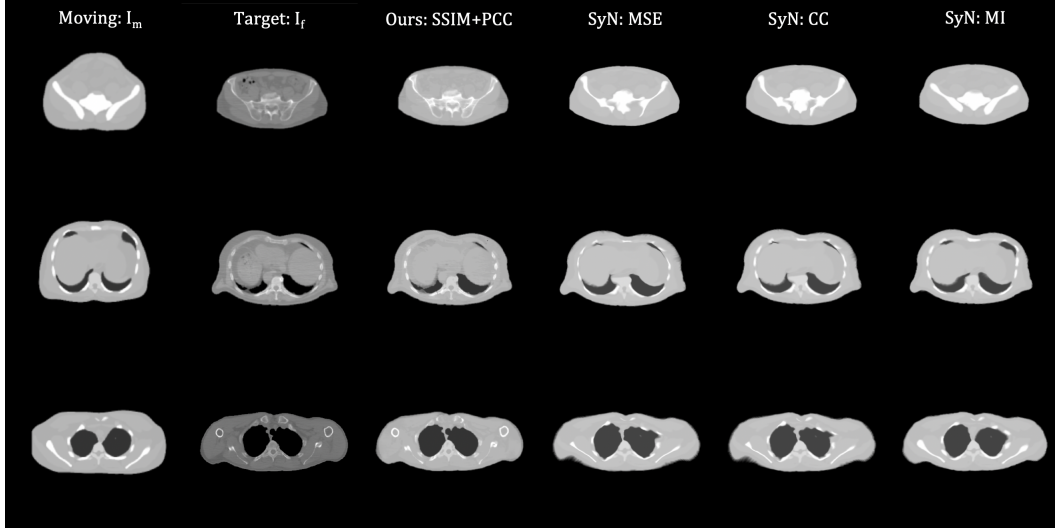


Fig. 5: Comparisons between our method and the SyN algorithm from the ANTs package. The 1st column: moving image (XCAT phantom). The 2nd column: target image (patient CT scan). The 3rd column: deformed moving image by the proposed method with SSIM+CC loss. The 4th column: deformed moving image by SyN with MSE. The 5th column: SyN with CC. The 6th column: SyN with MI.

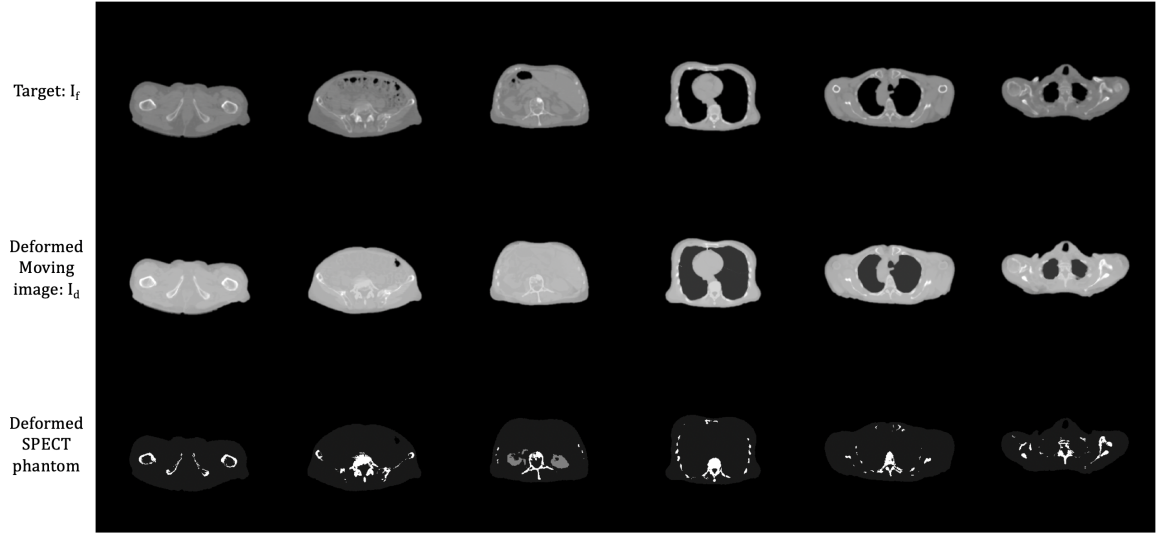


Fig. 6: Qualitative results from our method. The 1st row: target images. The 2nd row: deformed XCAT phantom. The 3rd row: deformed SPECT phantom.

Algorithm 1 ConvNet Registration

```

1: procedure CNNREG( $I_m, I_f$ )           ▷ Input  $I_m$  and  $I_f$ 
2:    $f_\theta = \text{Initialize}(\text{ConvNet})$ 
3:   while  $i < \text{iter}$  do             ▷ For  $\text{iter}$  number of iterations
4:      $\phi = f_\theta([I_m, I_f], I_f)$    ▷ Predict deformation,  $\phi$ 
5:      $I_d = I_m \circ \phi$                  ▷ Deform moving image,  $I_m$ 
6:      $\ell = \mathcal{L}(I_d, I_f; \theta)$      ▷ Compute loss
7:      $f_\theta = \text{BackPropagate}(f_\theta, \ell)$  ▷ Update ConvNet
8:   return  $I_d, \phi$ 
  
```

nine clinical low-dose whole-body CT patient scans used in this study; for those, only the torso part of the scans was extracted, which is 1153 2D-transaxial slices in total. The

data was obtained from a publicly available dataset (NaF Prostate, [37]) in the Cancer imaging archive (TCIA, [38]). We first compare the performance generated by the ConvNets with different image similarity metrics. Then, we compare the proposed method with a state-of-the-art registration algorithm, the symmetric image normalization method (SyN) [16] from the ANTs package [39].

A. Loss Function Comparisons

Some examples of the registered XCAT phantom image by the five loss functions were shown in Figure. 3. (a) and (h) represent a same moving image, and (b) and (i) are the target images from the same CT slice, where the later was blurred by a low-pass Gaussian filter due to the presence of beam

hardening artifacts. The third column to the last column are registration results by PCC, SSIM, PCC+SSIM, MSE, and CC, respectively. MSE and CC are two common loss functions in both traditional and learning-based image registration methods [14], [16], [18], [20]–[23], [34], but they failed to converge to good results (last two columns in Figure. 3). While PCC is robust to beam hardening artifacts, it produced an cartoonish contents around the spine (referring to (c) and (j)). On the other hand, SSIM completely models the noises and artifacts in the target image. The results produced by SSIM+PCC are much more balanced, combining with the Gaussian filter to additionally reduce noises, SSIM+PCC generated the best qualitative results among other loss functions.

Method	SSIM	MSE
Affine only	0.828 ± 0.008	69.213 ± 2.748
Ours	0.955 ± 0.007	37.340 ± 5.078
SyN (MSE)	0.884 ± 0.011	51.999 ± 4.135
SyN (MI)	0.881 ± 0.011	55.059 ± 3.996
SyN (CC)	0.886 ± 0.011	52.838 ± 4.138

TABLE I: Comparison of SSIM and MSE between the proposed and the SyN method, where the best performances were highlighted.

B. Registration Performance Comparisons

In this experiment, we compared the proposed method with the SyN algorithm [16]. Figure. 5 shows some qualitative comparisons between the proposed method and the SyN method. The first and the second columns indicate moving and fixed images. The third column shows the results generated by the proposed method. The fourth to the last columns represent the results obtained by SyN with MSE, CC, and MI, respectively. At a glance, our method gave a more accurate deformation than SyN, where the anatomy of bone structures and soft tissues were modeled precisely. Figure. 6 displays some qualitative results from the proposed method. The first row indicates the target images. The second and last rows show the deformed moving image and the deformed bone labels, respectively. Since the gold-standard is not available for the NaF Prostate dataset [37], the registration performances were evaluated quantitatively based on MSE and SSIM between $I_m \circ \phi$ and I_f . The results are shown in Table. I. The proposed method gave a mean SSIM of 0.947 and a mean MSE of 41.235, which outperformed the SyN method by a significant margin.

C. SPECT image simulations

Figure. 7 shows the results of mapping the XCAT phantom to a patient CT image. (a) and (b) exhibit the volume renderings of the phantom using 3DSlicer [40]. (c) and (d) show a coronal slice of the deformed phantom and the SPECT simulation, respectively. SPECT projections were simulated by an analytic projection algorithm that realistically models attenuation, scatter, and the spatially-varying collimator-detector response [41], [42]. SPECT images were reconstructed using a subsets expectation-maximization algorithm (OS-EM) [43] based method [44], with 2 iterations and 10 subsets.

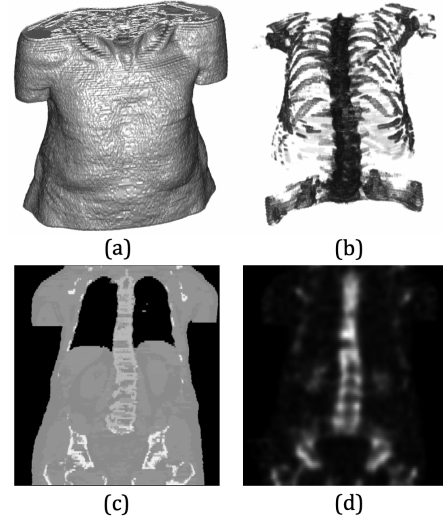


Fig. 7: Visualizations of deformed phantom and SPECT simulations. (a) Volume rendering of the deformed phantom. (b) Rendering of the skeleton. (c) A coronal slice of the phantom. (d) A coronal slice of the simulated SPECT image.

IV. CONCLUSION

This paper proposed to create patient-like phantoms with a ConvNet-based unsupervised and end-to-end registration technique that requires no prior training. Furthermore, we showed that the registration performance was significantly improved by combining SSIM and PCC as a data similarity loss function. The registration method was evaluated on the application of registering XCAT phantom with real patient CT scans and compared the registration performance in terms of SSIM and MSE to a state-of-the-art image registration method. Both quantitative and qualitative analysis indicate that our method provided the best results. Combined with Monte Carlo and CT simulation programs, the phantoms generated by our method are able to be transformed into more realistic human-like simulations.

ACKNOWLEDGMENT

This work was supported by a grant from the National Cancer Institute, U01-CA140204. The views expressed in written conference materials or publications and by speakers and moderators do not necessarily reflect the official policies of the NIH; nor does mention by trade names, commercial practices, or organizations imply endorsement by the U.S. Government.

We would like to show our gratitude to Dr. Daniel Tward and Shuwen Wei for sharing their pearls of wisdom with us during the course of this research.

REFERENCES

- [1] C. P. Christoffersen, D. Hansen, P. Poulsen, and T. S. Sorensen, "Registration-based reconstruction of four-dimensional cone beam computed tomography," *IEEE Transactions on Medical Imaging*, vol. 32, no. 11, pp. 2064–2077, 2013.

- [2] Y. Zhang, J. Ma, P. Iyengar, Y. Zhong, and J. Wang, "A new CT reconstruction technique using adaptive deformation recovery and intensity correction (ADRIC)," *Medical Physics*, vol. 44, no. 6, pp. 2223–2241, jun 2017. [Online]. Available: <http://doi.wiley.com/10.1002/mp.12259>
- [3] J. Chen, A. K. Jha, and E. C. Frey, "Incorporating CT prior information in the robust fuzzy C-means algorithm for QSPECT image segmentation," in *Medical Imaging 2019: Image Processing*, E. D. Angelini and B. A. Landman, Eds. SPIE, mar 2019, p. 66. [Online]. Available: <https://www.spiedigitallibrary.org/conference-proceedings-of-spie/10949/2506805/Incorporating-CT-prior-information-in-the-robust-fuzzy-C-means/10.1117/12.2506805.full>
- [4] M. Abdoli, R. A. J. O. Dierckx, and H. Zaidi, "Contourlet-based active contour model for PET image segmentation," *Medical Physics*, vol. 40, no. 8, p. 082507, jul 2013. [Online]. Available: <http://doi.wiley.com/10.1118/1.4816296>
- [5] W. P. Segars, G. Sturgeon, S. Mendonca, J. Grimes, and B. M. Tsui, "4D XCAT phantom for multimodality imaging research," *Medical Physics*, vol. 37, no. 9, pp. 4902–4915, 2010.
- [6] B. He, R. L. Wahl, Y. Du, G. Sgouros, H. Jacene, I. Flinn, and E. C. Frey, "Comparison of residence time estimation methods for radioimmunotherapy dosimetry and treatment planning-Monte Carlo simulation studies," *IEEE Transactions on Medical Imaging*, vol. 27, no. 4, pp. 521–530, apr 2008.
- [7] M. Ghaly, Y. Du, J. M. Links, and E. C. Frey, "Collimator optimization in myocardial perfusion SPECT using the ideal observer and realistic background variability for lesion detection and joint detection and localization tasks," *Physics in Medicine and Biology*, vol. 61, no. 5, pp. 2048–2066, feb 2016.
- [8] Y. Li, S. O'Reilly, D. Plyku, S. T. Treves, Y. Du, F. Fahey, X. Cao, A. K. Jha, G. Sgouros, W. E. Bolch, and E. C. Frey, "A projection image database to investigate factors affecting image quality in weight-based dosing: Application to pediatric renal SPECT," *Physics in Medicine and Biology*, vol. 63, no. 14, jul 2018.
- [9] K. Gong, J. Guan, C.-C. Liu, and J. Qi, "PET Image Denoising Using a Deep Neural Network Through Fine Tuning," *IEEE Transactions on Radiation and Plasma Medical Sciences*, vol. 3, no. 2, pp. 153–161, oct 2018.
- [10] K. Gong, J. Guan, K. Kim, X. Zhang, J. Yang, Y. Seo, G. El Fakhri, J. Qi, and Q. Li, "Iterative PET image reconstruction using convolutional neural network representation," *IEEE Transactions on Medical Imaging*, vol. 38, no. 3, pp. 675–685, mar 2019.
- [11] H. Lee, J. Lee, and S. Cho, "View-interpolation of sparsely sampled sinogram using convolutional neural network," in *Medical Imaging 2017: Image Processing*, vol. 10133. SPIE, feb 2017, p. 1013328.
- [12] W. P. Segars, J. Bond, J. Frush, S. Hon, C. Eckersley, C. H. Williams, J. Feng, D. J. Tward, J. T. Ratnanather, M. I. Miller, D. Frush, and E. Samei, "Population of anatomically variable 4D XCAT adult phantoms for imaging research and optimization," *Medical Physics*, vol. 40, no. 4, p. 043701, mar 2013. [Online]. Available: <http://doi.wiley.com/10.1118/1.4794178>
- [13] A. Sotiras, C. Davatzikos, and N. Paragios, "Deformable medical image registration: A survey," *IEEE Transactions on Medical Imaging*, vol. 32, no. 7, pp. 1153–1190, 2013.
- [14] M. F. Beg, M. I. Miller, A. Trounev, and L. Younes, "Computing large deformation metric mappings via geodesic flows of diffeomorphisms," *International Journal of Computer Vision*, vol. 61, no. 2, pp. 139–157, feb 2005.
- [15] G. Wolberg and S. Zokai, "Robust image registration using log-polar transform," in *Proceedings 2000 International Conference on Image Processing (Cat. No.00CH37101)*, vol. 1, Sep. 2000, pp. 493–496 vol.1.
- [16] B. B. Avants, C. L. Epstein, M. Grossman, and J. C. Gee, "Symmetric diffeomorphic image registration with cross-correlation: Evaluating automated labeling of elderly and neurodegenerative brain," *Medical Image Analysis*, vol. 12, no. 1, pp. 26–41, feb 2008.
- [17] P. Viola and W. M. Wells, "Alignment by Maximization of Mutual Information," *International Journal of Computer Vision*, vol. 24, no. 2, pp. 137–154, 1997.
- [18] G. Balakrishnan, A. Zhao, M. R. Sabuncu, J. Guttag, and A. V. Dalca, "VoxelMorph: A Learning Framework for Deformable Medical Image Registration," *IEEE Transactions on Medical Imaging*, vol. 38, no. 8, pp. 1788–1800, feb 2019.
- [19] D. Rueckert, P. Aljabar, R. A. Heckemann, J. V. Hajnal, and A. Hammers, "Diffeomorphic registration using B-splines," in *Lecture Notes in Computer Science (including subseries Lecture Notes in Artificial Intelligence and Lecture Notes in Bioinformatics)*, vol. 4191 LNCS. Springer Verlag, 2006, pp. 702–709.
- [20] A. V. Dalca, G. Balakrishnan, J. Guttag, and M. R. Sabuncu, "Unsupervised learning of probabilistic diffeomorphic registration for images and surfaces," *Medical Image Analysis*, vol. 57, pp. 226–236, oct 2019.
- [21] B. D. de Vos, F. F. Berendsen, M. A. Viergever, M. Staring, and I. Išgum, "End-to-end unsupervised deformable image registration with a convolutional neural network," *Lecture Notes in Computer Science (including subseries Lecture Notes in Artificial Intelligence and Lecture Notes in Bioinformatics)*, vol. 10553 LNCS, pp. 204–212, 2017.
- [22] G. Balakrishnan, A. Zhao, M. R. Sabuncu, A. V. Dalca, and J. Guttag, "An Unsupervised Learning Model for Deformable Medical Image Registration," in *Proceedings of the IEEE Computer Society Conference on Computer Vision and Pattern Recognition*, 2018, pp. 9252–9260. [Online]. Available: <https://github.com/balag/voxelmorph>
- [23] J. Krebs, H. Delingette, B. Mailhe, N. Ayache, and T. Mansi, "Learning a Probabilistic Model for Diffeomorphic Registration," *IEEE Transactions on Medical Imaging*, vol. 38, no. 9, pp. 2165–2176, feb 2019.
- [24] C. Zhang, S. Bengio, M. Hardt, B. Recht, and O. Vinyals, "Understanding deep learning requires rethinking generalization," *arXiv*, nov 2016. [Online]. Available: <http://arxiv.org/abs/1611.03530>
- [25] J. Su, D. V. Vargas, and K. Sakurai, "One Pixel Attack for Fooling Deep Neural Networks," *IEEE Transactions on Evolutionary Computation*, vol. 23, no. 5, pp. 828–841, jan 2019.
- [26] S. M. Moosavi-Dezfooli, A. Fawzi, and P. Frossard, "DeepFool: A Simple and Accurate Method to Fool Deep Neural Networks," in *Proceedings of the IEEE Computer Society Conference on Computer Vision and Pattern Recognition*, vol. 2016-December. IEEE Computer Society, dec 2016, pp. 2574–2582.
- [27] I. J. Goodfellow, J. Shlens, and C. Szegedy, "Explaining and Harnessing Adversarial Examples," *arXiv*, dec 2014. [Online]. Available: <http://arxiv.org/abs/1412.6572>
- [28] N. Papernot, P. McDaniel, S. Jha, M. Fredrikson, Z. B. Celik, and A. Swami, "The limitations of deep learning in adversarial settings," in *Proceedings - 2016 IEEE European Symposium on Security and Privacy, EURO S and P 2016*. Institute of Electrical and Electronics Engineers Inc., may 2016, pp. 372–387.
- [29] C. Szegedy, W. Zaremba, I. Sutskever, J. Bruna, D. Erhan, I. Goodfellow, and R. Fergus, "Intriguing properties of neural networks," *arXiv*, dec 2013. [Online]. Available: <http://arxiv.org/abs/1312.6199>
- [30] V. Lempitsky, A. Vedaldi, and D. Ulyanov, "Deep Image Prior," in *Proceedings of the IEEE Computer Society Conference on Computer Vision and Pattern Recognition*. IEEE Computer Society, dec 2018, pp. 9446–9454.
- [31] W. P. Segars, M. Mahesh, T. J. Beck, E. C. Frey, and B. M. Tsui, "Realistic CT simulation using the 4D XCAT phantom," *Medical Physics*, vol. 35, no. 8, pp. 3800–3808, 2008.
- [32] O. Ronneberger, P. Fischer, and T. Brox, "U-Net: Convolutional Networks for Biomedical Image Segmentation," *arXiv*, may 2015. [Online]. Available: <https://arxiv.org/abs/1505.04597>
- [33] Z. S. Saad, D. R. Glen, G. Chen, M. S. Beauchamp, R. Desai, and R. W. Cox, "A new method for improving functional-to-structural MRI alignment using local Pearson correlation," *NeuroImage*, vol. 44, no. 3, pp. 839–848, feb 2009.
- [34] W. Zhu, A. Myronenko, Z. Xu, W. Li, H. Roth, Y. Huang, F. Milletari, and D. Xu, "NeurReg: Neural Registration and Its Application to Image Segmentation," *arXiv*, oct 2019. [Online]. Available: <http://arxiv.org/abs/1910.01763>
- [35] Z. Wang, A. C. Bovik, H. R. Sheikh, and E. P. Simoncelli, "Image quality assessment: From error visibility to structural similarity," *IEEE Transactions on Image Processing*, vol. 13, no. 4, pp. 600–612, apr 2004.
- [36] L. A. Shepp and B. F. Logan, "FOURIER RECONSTRUCTION OF A HEAD SECTION," *IEEE Transactions on Nuclear Science*, vol. NS-21, no. 3, pp. 21–43, 1974.
- [37] K. A. Kurdziel, J. H. Shih, A. B. Apolo, L. Lindenberg, E. Mena, Y. Y. McKinney, S. S. Adler, B. Turkbey, W. Dahut, J. L. Gulley, R. A. Madan, O. Landgren, and P. L. Choyke, "The kinetics and reproducibility of 18F-sodium fluoride for oncology using current PET camera technology," *Journal of nuclear medicine : official publication, Society of Nuclear Medicine*, vol. 53, no. 8, pp. 1175–84, aug 2012. [Online]. Available: <http://www.ncbi.nlm.nih.gov/pubmed/22728263http://www.pubmedcentral.nih.gov/articlerender.fcgi?artid=PMC3474293>
- [38] K. Clark, B. Vendt, K. Smith, J. Freymann, J. Kirby, P. Koppel, S. Moore, S. Phillips, D. Maffitt, M. Pringle, L. Tarbox, and F. Prior, "The cancer imaging archive (TCIA): Maintaining and operating a public information repository," *Journal of Digital Imaging*, vol. 26, no. 6, pp. 1045–1057, dec 2013.

- [39] B. B. Avants, N. J. Tustison, G. Song, and J. C. Gee, "ANTS: Open-source tools for normalization and neuroanatomy," *IEEE Transactions on Biomedical Engineering*, vol. 10, pp. 1–11, 2009. [Online]. Available: <ftp://ftp.heanet.ie/mirrors/sourceforge/a/ad/advants/Documentation/antstheory.pdf>
- [40] A. Fedorov, R. Beichel, J. Kalpathy-Cramer, J. Finet, J.-C. Fillion-Robin, S. Pujol, C. Bauer, D. Jennings, F. Fennessy, M. Sonka, J. Buatti, S. Aylward, J. V. Miller, S. Pieper, and R. Kikinis, "3d slicer as an image computing platform for the quantitative imaging network," *Magnetic Resonance Imaging*, vol. 30, no. 9, pp. 1323 – 1341, 2012, quantitative Imaging in Cancer. [Online]. Available: <http://www.sciencedirect.com/science/article/pii/S0730725X12001816>
- [41] E. C. Frey and B. M. W. Tsui, "A practical method for incorporating scatter in a projector-backprojector for accurate scatter compensation in spect," *IEEE Transactions on Nuclear Science*, vol. 40, no. 4, pp. 1107–1116, Aug 1993.
- [42] D. J. Kadrmas, E. C. Frey, and B. M. W. Tsui, "An svd investigation of modeling scatter in multiple energy windows for improved spect images," *IEEE Transactions on Nuclear Science*, vol. 43, no. 4, pp. 2275–2284, Aug 1996.
- [43] H. M. Hudson and R. S. Larkin, "Accelerated image reconstruction using ordered subsets of projection data," *IEEE Transactions on Medical Imaging*, vol. 13, no. 4, pp. 601–609, Dec 1994.
- [44] B. He, Y. Du, X. Song, W. P. Segars, and E. C. Frey, "A Monte Carlo and physical phantom evaluation of quantitative In-111 SPECT," *Physics in Medicine and Biology*, vol. 50, no. 17, pp. 4169–4185, sep 2005.